1990-04-01

Phase locking in an infrared short-pulse free-electron laser

Oepts, D.; Colson, W.B.

Journal Name: IEEE Journal of Quantum Electronics (Institute of Electrical and Electronics Engineers); (USA); Journal Volume: 26:4
http://hdl.handle.net/10945/61056

Phase Locking in an Infrared Short-Pulse Free-Electron Laser

D. OEPTS AND W. B. COLSON

Abstract—**In a free-electron laser operating in the infrared and far-infrared spectral regions and using a radio-frequency accelerator for the electron beam, the electron pulse length can be of the same order as the slippage length or even shorter. Such a laser emits short pulses of multimode broad-band radiation. If the repetition time of the electron pulses is short compared to the round-trip time of an optical pulse in the resonator cavity, then phase locking between successive optical pulses can be induced by an intracavity interferometric device. This causes a reduction of the number of active cavity modes, and leads to a significant increase in the power per mode. External selection of a single mode with reasonable power then becomes possible.**

The feasibility of the phase-locking procedure has been tested by simulation of the optical pulse evolution in a short-pulse free-electron laser, using a model based on the self-consistent solution of the equations of motion for the electrons and the wave equation driven by single-particle currents.

The simulations show that a high degree of coherence between successive pulses can be induced by a low-finesse etalon. Saturated operation in a greatly reduced number of modes, but with the same total power, is attained with a slight delay in the growth of the power as compared to the case without phase locking.

I. Introduction

OPERATION in a single cavity mode is desirable for spectroscopic applications of a laser. Due to the long cavity and the broad gain bandwidth, a free-electron laser (FEL) can oscillate in a very large number of cavity modes. The homogeneous bandwidth usually exceeds the inhomogeneous one, and mode competition can cause a narrowing of the spectrum as in other lasers. The final width is determined by the quality factor of the cavity, by external sources of noise, and by the duration of the pulse. For short pulses, the latter effect dominates and the resulting spectral width is said to be transform limited. A radio-frequency accelerator produces electrons in micropulses with a duration in the picosecond range. In an FEL based on such an accelerator, many modes are coupled due to the short pulse length.

Manuscript received June 6, 1989; revised October 31, 1989. This work was performed as part of the research program of the association agreement between Euratom and the "Stichting voor Fundamenteel Onderzoek der Materie" (FOM) with financial support from the "Nederlandse Organisatie voor Wetenschappelijk Onderzoek" (NWO) and Euratom.

D. Oepts is with the FOM-Instituut voor Plasmafysica "Rijnhuizen," Association Euratom-FOM, Edisonbaan 14, 3439 MN Nieuwegein, The Netherlands.

W. B. Colson was with Berkeley Research Associates, Inc., Berkeley, CA 94701. He is now with the Department of Physics, Naval Postgraduate School, Monterey, CA 93940.

IEEE Log Number 8933821.

A characteristic parameter for a free-electron laser is the slippage length $N\lambda_s$ where N is the number of undulator periods and λ_s is the wavelength of the radiation. It gives the difference between the distances traveled by an electron and by an optical wavefront, respectively, in the transit time for an electron through the undulator. The homogeneous gain bandwidth of a free-electron laser is determined by the slippage length: $\Delta\nu_g = c/2N\lambda_s$. The Fourier transform limit for the bandwidth is given by $\Delta\nu = 1/T_\mu$ where T_μ is the duration of the light micropulse. For electron pulses long compared to the slippage length, the optical pulse length is almost equal to the electron pulse length. For short electron pulses, the optical pulse length is on the order of the slippage length. In that case, the transform limit is as wide as the gain bandwidth so that no narrowing is possible. Instead of mode competition, there is mode coupling, and the FEL operates as a synchronously pumped mode-locked laser. In order to increase the power available in a narrow line, it is proposed to use an intracavity interferometric device to reduce the number of active cavity modes. The principle of the method is discussed in Section II-B. Numerical simulations to test the feasibility of the procedure are described in Section III-B.

II. Theory

A. Pulse Evolution

The optical pulse evolution has been studied with the model developed by Colson [1]–[3]. The method is based on the self-consistent solution of the coupled Maxwell–Lorentz equations for the optical wave and for the electron motion. The electromagnetic field is written as a carrier wave $e^{i(k_s z - \omega_s t)}$, with a time-dependent complex amplitude. It is assumed that the amplitude and the phase of the wave, and the macroscopic density of the electrons, vary little over a wavelength of the optical field. A number of dimensionless parameters is defined to bring the equations in a convenient form. The dimensionless time is $\tau = ct/L_u$ and the dimensionless z coordinate is $\tilde{z} = z/N\lambda_s$ where L_u is the length of the undulator and λ_s is the wavelength of the carrier. The dimensionless complex wave amplitude is defined by $a = |a|e^{i\phi}$ with

$$|a| = 4\pi NeEKL_u/\gamma^2 mc^2 \qquad (1)$$

where E is the electric field strength, $K = eB\lambda_u/2\pi mc^2$ is the undulator strength parameter, B is the (rms) un-

dulator field strength, e and m are the electron charge and mass, c is the velocity of light in vacuum, and γ is the Lorentz factor of the electrons. The dimensionless macroscopic electron current density is

$$j = 8N(e\pi KL_u)^2\rho/4\pi\epsilon_0\gamma^3mc^2 \quad (2)$$

where ρ is the electron density. The electron phase ζ is defined as $\zeta = (k_s + k_u)z(t) - \omega_s t$ where $k_u = 2\pi/\lambda_u$, λ_u being the undulator period. With the assumptions $N \gg 1$, $\gamma \gg 1$, and λ_s not too far from the resonance wavelength $\lambda_r = \lambda_u(1 + K^2)/2\gamma^2$, the equation for the longitudinal electron motion can be written in the form of the pendulum equation

$$\frac{\partial^2\zeta(z + \tau)}{\partial\tau^2} = \left|a(z, \tau)\right| \cos\left(\zeta(z + \tau) + \phi(z)\right), \quad (3)$$

while the change in the wave field due to the electron currents is given by

$$\frac{\partial a(z, \tau)}{\partial\tau} = -j(z + \tau)\langle e^{-i\zeta(z+\tau)}\rangle. \quad (4)$$

The angle brackets denote averaging over the electrons at the macroscopic position $z + \tau$. The electrons are characterized by their initial conditions. We have dropped the tilde from the dimensionless position coordinate $\tilde{z}$ in (3) and (4) and in the rest of this paper. The equations are valid for low and high gain and in weak and strong fields.

Equations (3) and (4) do not contain a spatial dependence in the transverse directions. A generalization is possible to include diffraction effects of the optical wave and transverse motion of the electrons due to the finite emittance of the electron beam and the inhomogeneity of the undulator field. However, as the phase-locking and short-pulse effects essentially relate to longitudinal structure only, the one-dimensional formulation has been used in the present work. The effects of electron beam quality and optical diffraction have been taken into account by using a reduced effective j value. The weak-field theory [4] has been used to determine the gain degradation due to electron beam emittance and energy spread. The effective overlap between the electron beam and the optical beam is represented by a geometrical filling factor (see Section III-A).

To simulate the optical pulse evolution, an electron pulse with current profile $j(z)$ is injected into the undulator at $\tau = 0$, and its interaction with the optical pulse produced in earlier passes is calculated by numerically solving (3) and (4) for a number of z positions in the optical wave in a series of steps in time τ. The phasing between the optical pulse and the new electron pulse is such that desynchronism can be accounted for, i.e., we allow the repetition time of the electron pulses to be different from the round-trip time of the optical pulses in the cavity.

The initial phases of the sample electrons in each pulse are distributed essentially uniformly over the range $-\pi$ to $+\pi$. A small random variation is added to each electron phase, however, to represent spontaneous density fluctuations in the beam, so that a random spontaneous contribution to the optical field is generated, and no initial correlation between the electron pulses is introduced. This is important in studying the development of coherence.

For each electron pulse, the average in (4) is initially practically zero; the optical gain builds up only during the passage through the undulator. The leading part of the optical pulse is, therefore, not amplified in the case of perfect synchronism. In effect, the optical pulse shifts to the back of the electron pulse and the net gain diminishes [5], [6]. This lethargy effect can be partly compensated by introducing a suitable desynchronism between the optical pulse and the electron pulse. In a strong optical field, the predominance of the power increase at the trailing end of the optical pulse is reduced due to saturation. Therefore, the desynchronization needed to obtain optimum strong-signal gain and maximum saturated power is smaller than the optimum in the small-signal case. A desynchronization that is a reasonable compromise between initial gain and final saturated power has been chosen in the simulations.

B. Spectral Structure and Phase Locking

A radio-frequency linear accelerator (RF linac) produces an electron beam in the form of macropulses with a duration in the microsecond range, each consisting of a series of micropulses in the picosecond range. The temporal and spectral structure of the optical pulses generated by an RF-linac-based free-electron laser are illustrated in Fig. 1 at different time and frequency scales. In Fig. 1(a), the form of the macropulses is sketched: t_0 is the start of the electron beam macropulse, at t_1 saturation is reached, at t_2 the electron pulse ends, and the laser power rings down with a decay time corresponding to the cavity Q factor. Fig. 1(b) shows a part of Fig. 1(a) in more detail: the pulse is built up out of very short micropulses spaced by T_r. The power shows a periodic structure corresponding to the round-trip time $T_c = 2L_c/c$ for a light pulse through the cavity of length L_c. In Fig. 1(c), the shape of the micropulses is sketched, and for completeness, the electromagnetic field oscillations are indicated in Fig. 1(d).

The right half of Fig. 1 shows the corresponding spectral structure in increasing detail from bottom to top: Fig. 1(h) gives the overall spectrum shape, with a width corresponding to T_μ and center frequency ν_s. In Fig. 1(g), the spectrum is seen on an expanded scale. Fig. 1(f) shows the structure corresponding to the periodicity in Fig. 1(b), i.e., the cavity modes. Finally, Fig. 1(e) indicates the shape of the individual cavity modes, with a width given by the correlation time in Fig. 1(a), i.e., the cavity decay time. Only the longitudinal mode structure is considered here; we assume that higher order transverse modes are suppressed by a suitable resonator configuration.

The number of cavity modes within the gain profile is determined by the cavity length and by the slippage length. For a cavity of length L_c, the mode spacing is $\Delta\nu_c = c/2L_c$. The minimum cavity length is equal to the un-

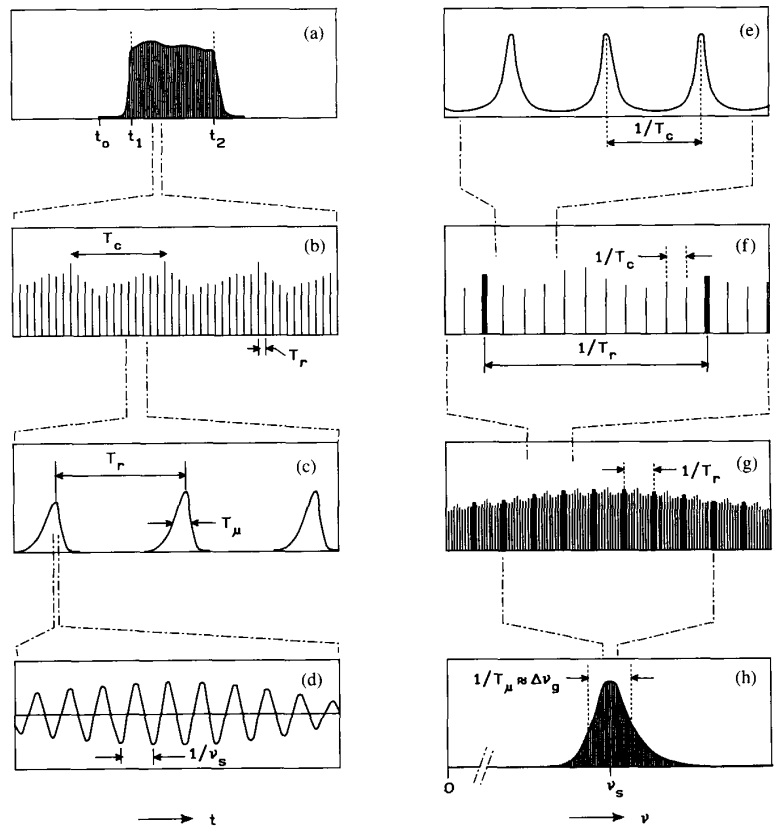

Fig. 1. Structure of light pulses from an RF-linac-based FEL at different time scales and the corresponding spectral structure. See text for explanation.

dulator length: $L_c \geq N\lambda_u$. The gain bandwidth $\Delta\nu_g$ is at least equal to the homogeneous width determined by the number of undulator periods N: $\Delta\nu_g \geq \nu_s/2N$. For the number of cavity modes within the gain bandwidth, we thus have

$$m_g = \frac{\Delta\nu_g}{\Delta\nu_c} \geq \frac{\nu_s}{2N}\frac{2L_c}{c} = \frac{\lambda_u}{\lambda_s}. \tag{5}$$

As $\lambda_s \approx \lambda_u/\gamma^2$, we thus have $m_g > \gamma^2$, and many thousands of cavity modes can be excited simultaneously.

When the optical pulse is as short as the slippage length $N\lambda_s$, all these modes are coupled and the spectrum is broad and almost continuous. In the short-pulse, long-wavelength case, the spectral width can be reduced only when the optical pulse length is made longer than the slippage length. Desynchronization can be applied to achieve pulse stretching to a certain extent. Although the FEL efficiency decreases with increasing desynchronization, the spectral power density increases as long as the growth of the coherence length outweighs the power decrement. The spectral narrowing that can be obtained this way depends on the cavity losses and on the available gain. For the case considered in Section III, for example, a narrowing by a factor of two or three is possible.

We now consider a possibility to substantially reduce the number of active modes within the fixed bandwidth determined by the slippage length. If the interval T_r between pulses is short compared to the cavity round-trip time T_c, then there is a large number m_c of light pulses present in the cavity at any time. As an example, when L_c = 6 m and $1/T_r$ = 1 GHz, one has m_c = 40. Normally, these pulses are completely independent, and the power spectrum of the series of pulses is the same as if there were only one pulse circulating with m_c times the power. The situation is different when there is coherence between successive pulses. In the limit that all pulses are identical and coherent, the spectrum contains only multiples of the repetition frequency $1/T_r$, and the number of active modes is reduced by the factor m_c. The remaining modes are indicated in Fig. 1(f) by the heavier drawn vertical lines. The spectrum is identical to that of a laser having the cavity length $\frac{1}{2}cT_r$, and the laser may be said to be "supersynchronously pumped."

The required coherence can be induced by an interferometric device such as a slightly tilted etalon with a spacing adjusted to the pulse repetition rate so that the pulse circulating in the etalon overlaps with successive new pulses. In a steady-state view, the etalon acts as a filter transmitting only the selected modes [7]. As the total

length of the electron macropulse is limited, however, the steady state might not be attained when an etalon is present. In the initial phase, when the pulses are not yet coherent, the etalon rejects most of the radiation, and the growth of the laser power is impeded. It is, therefore, necessary to study the time-dependent behavior of the system.

C. Simulation of Phase Locking

Previous studies of the startup and multimode behavior of free-electron lasers [5], [8], [9] have been restricted to a single pulse in the cavity. Multiple independent pulses are covered by the same treatment, but no theory is available for the case where multiple pulses interact. Therefore, the simulation procedure described in Section II-A has been extended to treat the case of multiple pulses in the cavity together with an etalon.

Instead of, as usual, cycling only a single optical pulse repeatedly through the undulator, together with a "fresh" electron pulse at every pass, we now keep track of a number m_c of separate pulses $a_k(z)$.

The effect of the etalon is included in the following way. The optical field in the etalon is represented by a complex dimensionless amplitude $a_e(z)$, analogous to the amplitude $a_k(z)$ of the circulating pulses. After each pass through the undulator, the optical pulses are passed through the etalon according to the algorithm

$$a_e(z) := a_e(z) + t_1 a_k(z) \tag{6a}$$

$$a_k(z) := t_2 a_e(z) \tag{6b}$$

$$a_e(z) := r_2 r_1 a_e(z + 2L_e) = r_1 r_2 e^{i\phi_e} a_e(z + \delta). \tag{6c}$$

Here, $t_{1,2}$ and $r_{1,2}$ are the (possibly complex) amplitude transmission and reflection coefficients of the etalon mirrors. In (6a), the pulse amplitude transmitted by the first etalon mirror is added to the field already present in the etalon (the reflected part of a_k is lost due to the etalon tilt). In (6b), the amplitude transmitted by the second etalon mirror replaces the amplitude of the original pulse a_k. In (6c), the field in the etalon to which the next pulse will be added is found by reflection at both etalon mirrors. $\phi_e = 2\pi \times 2L_eN$ is the phase shift corresponding to the etalon spacing L_e in units $N\lambda_s$. When the etalon spacing is an integer fraction of the cavity length, so that all etalon modes coincide with cavity modes, the factor $e^{i\phi_e}$ is unity and δ is zero. This will normally be the case, but detuning of the etalon can be used to stretch the pulses in a similar way as cavity detuning. In order to avoid the beam walk-off and the double-pass loss of a tilted transmission etalon, an alternative configuration like the Fox-Smith interferometer [10] would probably be used in practice. This situation can also be handled with (6), however.

III. Simulation Results

A. Pulse Evolution, Desynchronism, and Gain

In the simulations that have been performed, we have used parameters relevant to the Free Electron Laser for Infrared Experiments (FELIX), which is under construction at the FOM Institute for Plasmaphysics Rijnhuizen [11], [12]. The FELIX project involves the construction of a free-electron laser facility operating in the near infrared to millimeter-wave spectral regions. In the first stage of the project, a 3 GHz radio-frequency linear accelerator will be used to provide electrons with energies between 15 and 45 MeV in pulses with a peak current of 70 A, a duration of 3 ps, a repetition frequency of 1 GHz, and a macropulse length of 20 μs. Radiation with wavelengths in the 8–80 μm range will be produced. The undulator has 38 periods of 65 mm wavelength. With these parameters, the slippage length $N\lambda_s$ is equal to the electron micropulse length for $\lambda_s \approx 24$ μm. Simulations of the phase locking by an etalon have been performed for $\lambda_s = 25$ μm.

The basic parameters of the FELIX device are rather similar to those of the FEL operated successfully at the Los Alamos National Laboratory [13]. In the latter, however, there is just one pulse at a time present in the cavity, and so the phase-locking procedure discussed here is not applicable.

The value of j as given by (2) applies for a helical undulator; for a linear undulator, j is reduced by a factor depending on K [2]. For the energy spread parameter, expressed as $\sigma_e = 4\pi N\sigma_\gamma/\gamma$ where σ_γ is the standard deviation in γ, we have used $\sigma_e = 1.7$, while the normalized (rms) emittance is taken to be 50π mm · mrad. The gain degradation due to the energy spread and the emittance of the electron beam, as calculated from the weak-field theory [4], corresponds to a reduction of j by a factor of 1.8. A filling factor is determined by assuming for the optical beam a fundamental Gaussian mode with Rayleigh length $L_R = \frac{1}{3}L_u = 0.82$ m, while the electron beam is assumed to have an rms radius of 0.5 mm. Including the effects of the filling factor, the linear undulator, and the electron beam quality, one arrives at an effective peak value of $j = 7.5$ for the dimensionless current density. A parabolic shape with a full width at half maximum $l_e = 0.9$ mm has been used for the longitudinal electron density distribution.

A desynchronization of $d = \Delta L_c/N\lambda_s \approx 0.015$ where ΔL_c is the shortening of the optical round-trip path length was found to give a reasonable compromise between initial gain and final power. In this case, saturation is reached in roughly 200 passes, i.e., 8 μs for a cavity length of 6 m, with a peak dimensionless field strength $|a|$ between 50 and 100, and a dimensionless pulse length of approximately 1. The corresponding peak output power, at 3% outcoupling, is on the order of 10 MW, and the total energy in a micropulse is ≈ 60 μJ. With an assumed loss and outcoupling of 4.5%, the net small-signal gain was found to be $\approx 20\%$.

B. Phase Locking and Spectra

1) Multiple Pulse Simulation: An example of simulations with multiple pulses and phase locking is given in Figs. 2 and 3. The number of pulses is limited by the

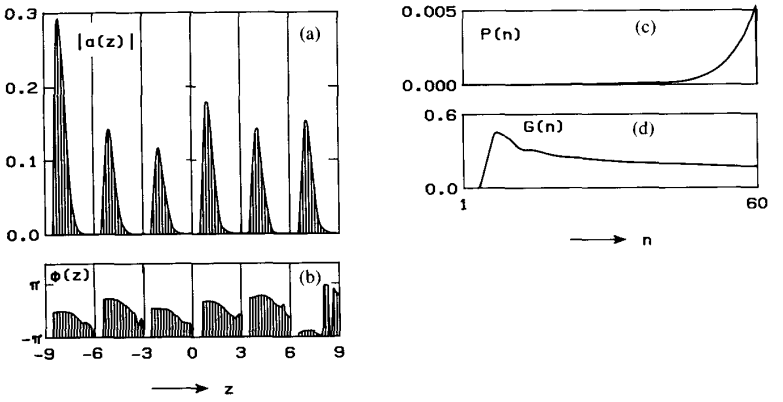

Fig. 2. Simulation result of amplitudes (a) and phases (b) in six independent pulses after 60 round-trips through an FEL with parameters corresponding to FELIX at 25 μm wavelength: effective j, taking beam quality effects into account: $j = 7.5$, cavity detuning $0.015N\lambda_s$, pulse length full-width-half-maximum $\sigma_z = 0.9N\lambda_s$, cavity loss and outcoupling 5%. The energy per pulse (c) and gain per pass (d) are shown as functions of the number of passes.

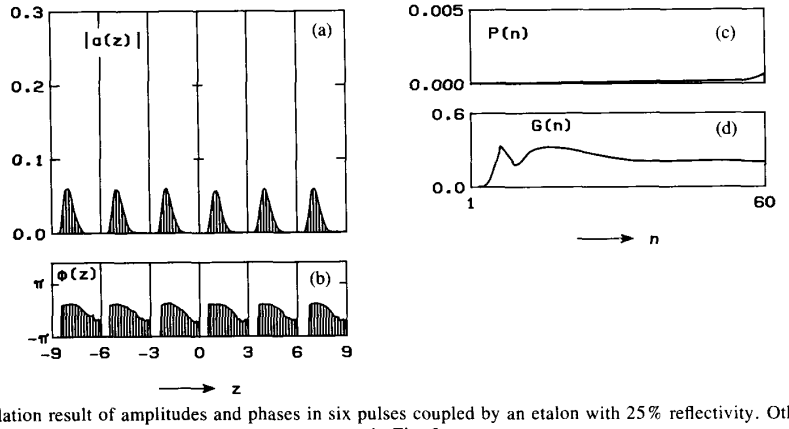

Fig. 3. Simulation result of amplitudes and phases in six pulses coupled by an etalon with 25% reflectivity. Other parameters as in Fig. 2.

computer facilities available at the time, but suffices to establish the basic principles of operation. The widely spaced pulses have been drawn close together for convenience. Fig. 2 shows the situation after 60 round-trips through the cavity without the phase-locking etalon. As the pulses have evolved independently out of the spontaneous noise, their amplitudes and phases are different, although the shapes of the different pulses are similar both in phase and amplitude. The right half of the figure shows the energy in the pulses and the energy gain per pass as a function of the number of passes. In Fig. 3, the simulation is shown for the case with an etalon. A reflectivity $r_{1,2}^2 = 25\%$ for both mirrors has been used. The etalon is exactly tuned to the optical pulse separation. Again, 60 full round-trips have been made. The pulses now have practically identical amplitude and phase profiles, both in shape and magnitude. Therefore, the spectrum contains only the modes corresponding to the pulse spacing T_r. The power is lower than in Fig. 2, due to the increased losses in the initial 10–20 passes. After about 20 passes, however, the pulses have become coherent, and the power gain per pass is the same as in the case without etalon. To simplify the comparison, absorption in the etalon mirrors has not been included in this example. When 1% absorption in each mirror is assumed, the cavity loss is increased by 2.6%, but the overall picture does not change.

2) Simple Pulse Evolution Model: The simulation described in the previous section has shown that all pulses rapidly acquire a similar shape, even without the etalon. Therefore, it is possible to use a simpler model in which each pulse is characterized by a single complex amplitude a_k. This makes it possible to keep track of a larger number of pulses and to show clearly the mode structure in the spectrum. Instead of considering the interaction between light and electrons in detail, we now simply assume that, on passing through the undulator, the amplitude of the pulse is multiplied by a gain factor Γ and that a spontaneous contribution with random phase and (Gaussian) random power is added. Saturation is described by assuming that the incremental power gain $G = \Gamma^2 - 1$ depends

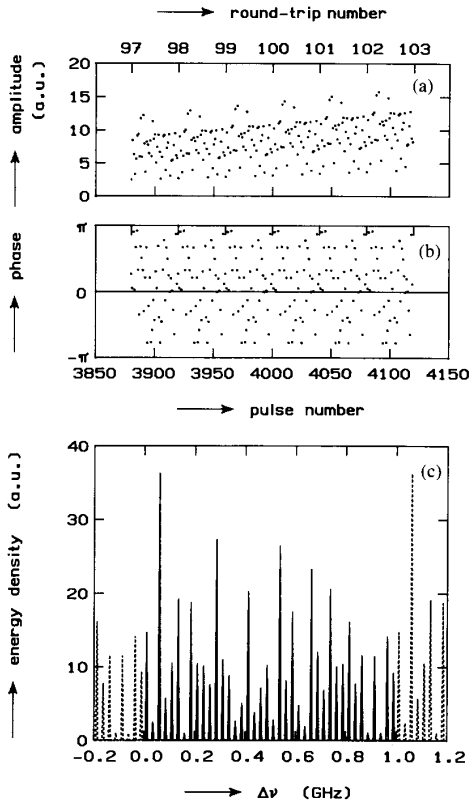

Fig. 4. Simulation result of amplitude (a) and phase (b) for 240 successive pulses after ≈ 100 full round-trips with 40 separate pulses in the cavity. Parameters: gross gain $G_0 = 25\%$, cavity loss and outcoupling 5.5%, $1/T_r = 1$ GHz, $L_c = 6$ m, $I_s = 10^8 \times I_{\text{spontaneous}}$. (c) The power spectrum corresponding to the series of pulses shown in (a) and (b).

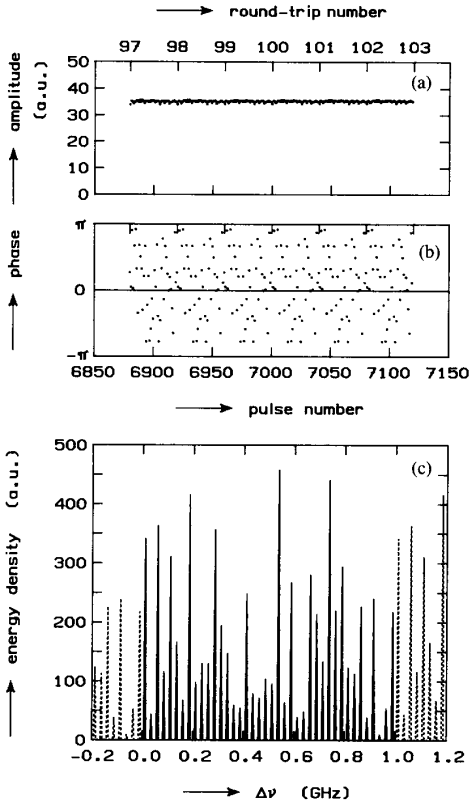

Fig. 5. Amplitude, phase, and spectrum for 240 pulses as in Fig. 4, after 75 more round-trips. Saturation has set in, and the amplitudes have almost reached their maximum values.

on the pulse power I_k as

$$G = \frac{G_0 I_s}{G_0 I_k + I_s}$$

where G_0 is the small-signal power gain and I_s is the maximum power increment. The etalon is incorporated in the same way as above, but now the field in the etalon is also represented by a single value. As the shape of the individual pulses is left unspecified, the corresponding spectral structure—cf. Fig. 1(c) and (d)—is also undetermined. The fine structure, on the other hand, is determined by the long-range pulse-to-pulse correlations—cf. Fig. 1(b), (e)—and can be found from the Fourier transform of the series of a_k values. As the a_k's are sampled with the interval T_r, the corresponding spectrum is periodic with $1/T_r$. Thus, one of the frequency intervals of width $1/T_r$—Fig. 1(f)—is sufficient to represent the main features of the mode structure. This interval is also the free spectral range of the etalon.

Examples of simulation results are shown in Figs. 4–7. Fig. 4(a), (b) give the amplitudes and phases of 240 pulses at $t \approx 4$ μs, i.e., after 100 round-trip times, without etalon. The periodic structure with a period of 40 pulses, corresponding to the cavity round-trip time, is apparent. Within each group of 40 pulses, there is no correlation. One $1/T_r$ period of the energy spectrum of this sequence of pulses is illustrated in Fig. 4(c) and shows the cavity modes. When saturation is reached, at about 6 μs with the parameters used, the pulse amplitudes become equal, but the phases remain random and the spectrum is basically unchanged, as illustrated in Fig. 5.

Fig. 6 shows the result with an etalon having mirrors with 25% reflectivity and 75% transmissivity (finesse = 2.1, peak transmission = 0.97). The 40-pulse periodicity is again visible, but now there is a large degree of coherence between successive pulses. This is reflected in the spectrum, Fig. 6(c), where the cavity modes in between the etalon modes are largely suppressed. The amplitude and phase modulations that are still present in Fig. 6(a) and (b) correspond to the remaining satellites around the etalon modes. The net gain is reduced by ≈3% due to the etalon mirror absorption, and as in Section III-B1), the initial growth is retarded for 10–20 roundtrips. As a result of both effects, saturation is reached some 2 μs later in this case than without the etalon. For a macropulse length of 20 μs, as in FELIX, this leaves more than 10 μs of saturated operation.

With a higher finesse etalon, a higher degree of coherence is reached, but the initial power growth is delayed

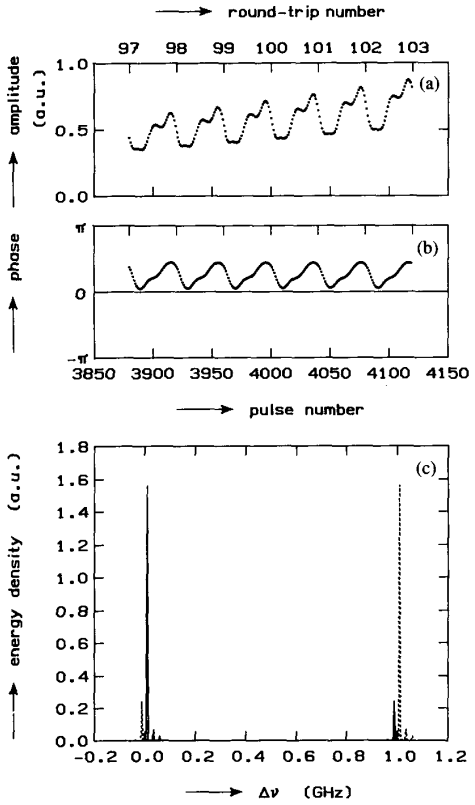

Fig. 6. Amplitude, phase, and spectrum for 240 successive pulses after 100 round-trips as in Fig. 4, with an etalon having mirrors with 25% reflectivity and 74% transmissivity.

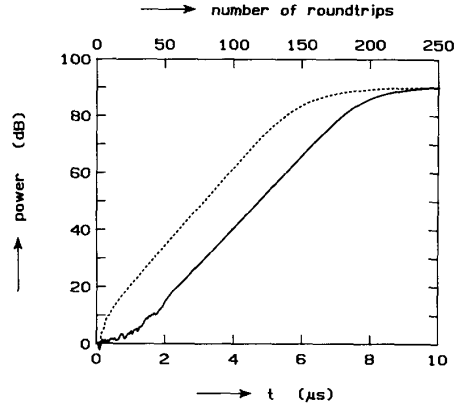

Fig. 7. Effect of a lossless etalon on the growth of the energy per micropulse. For clarity, an etalon with finesse = 11 has been assumed. Full line: with etalon; dashed line: without etalon.

more. Fig. 7 illustrates the power growth. To show this effect of an etalon more clearly, a mirror reflectivity of 75% and no absorption is used (finesse = 11). With etalon, the net power gain is low initially, but it equals that without etalon after 1.8 μs. This is the time needed to establish a degree of coherence between pulses such that the etalon transmission approaches unity.

With the etalon, the final energy per pulse is the same as without the etalon, and so the full output power is concentrated in the etalon modes. From the spectrum with a reduced number of well-separated modes, it is possible to select a single mode with an external filter or monochromator, or by selective outcoupling. The power in the selected mode depends on the total number of etalon modes within the laser bandwidth, which is on the order of 100 for the parameters used here.

It has been assumed in the simulations that all electron micropulses have identical shape and energy distribution, and that the repetition rate is perfectly constant. In practice, some jitter in the arrival times of the pulses will usually be present, as well as random and systematic variations in their energy. Time jitter can have an effect on the power gain and on the shape of the optical pulse due to the lethargy. The optical phase, however, is determined by the incoming optical signal and is not influenced by the precise position of the electron pulse. Variations of the electron energy affect the operation of the laser through a broadening and shift of the gain profile. This will be reflected in the overall shape of the spectrum illustrated in Fig. 1(h). The fine structure in the spectrum, however, is determined by the optical cavity and the etalon. In particular, the position and the width of the selected etalon modes depend only on the spacing and the quality of the etalon. Variations in the electron beam will therefore affect only the relative intensities of the active modes.

IV. Conclusions

Pulse evolution simulations have shown that the parameters of the FELIX project will enable it to function in the short-pulse regime where the electron pulse length is as short as the slippage length.

Simulations including the coupling of pulses by an intracavity interferometric device have shown that it is possible to induce coherence between otherwise independent pulses in an RF-linac FEL. Apart from an initial delay in the growth of the power and a gain reduction due to absorption loss, the basic operation of the FEL is unaffected.

A simple model for the simulation of the effect of an intracavity etalon on the spectral structure has shown that a low-finesse etalon suffices to suppress most of the cavity modes and to concentrate the power in modes with a much larger frequency separation.

Intracavity etalons or equivalent interferometric elements are commonly used in conventional lasers to reduce the spectral bandwidth. The application discussed here differs in that the free spectral range of the etalon is much narrower than the full gain bandwidth, and a sufficient number of etalon modes remains present to compose the short pulses.

References

[1] W. B. Colson and S. K. Ride, "The nonlinear wave equation for free electron lasers driven by single-particle currents," *Phys. Lett.*, vol. 76A, pp. 379-382, 1980.

[2] W. B. Colson, "Tutorial on classical free electron laser theory," *Nucl. Instrum. Methods*, vol. A237, pp. 1-9, 1985.
[3] ——, "Fundamental free electron laser theory and new principles for advanced devices," in *Free Electron Lasers: Critical Review of Technology*, B. E. Newnam, Ed., *Proc. SPIE*, vol. 738, 1988, pp. 2-72.
[4] W. B. Colson and J. Blau, "Free electron laser theory in weak optical fields," *Nucl. Instrum. Methods*, vol. A259, pp. 198-202, 1987.
[5] H. Al-Abawi, F. A. Hopf, G. T. Moore, and M. O. Scully, "Coherent transients in the free-electron laser: Laser lethargy and coherence brightening," *Opt. Commun.*, vol. 30, pp. 235-238, 1979.
[6] F. A. Hopf, Th. G. Kuper, G. T. Moore, and M. O. Scully, "The free-electron laser from a laser-physics perspective," in *Physics of Quantum Electronics, Vol. 7*, S. F. Jacobs *et al.*, Ed. Reading, MA: Addison Wesley, 1980, pp. 31-87.
[7] M. Hercher, "Tunable single mode operation of gas lasers using intracavity tilted etalons," *Appl. Opt.*, vol. 8, pp. 1103-1106, 1969.
[8] G. Dattoli, A. Marino, and A. Renieri, "A multimode small signal analysis of the single pass free electron laser," *Opt. Commun.*, vol. 35, pp. 407-412, 1980.
[9] P. Sprangle, C. M. Tang, and I. Bernstein, "Evolution of spontaneous and coherent radiation in the free-electron-laser oscillator," *Phys. Rev. A*, vol. 28, pp. 2300-2309, 1983.
[10] P. W. Smith, "Mode selection in lasers," *Proc. IEEE*, vol. 60, pp. 422-440, 1972.
[11] P. W. van Amersfoort, R. W. B. Best, B. Faatz, C. A. J. van der Geer, W. J. Mastop, B. J. H. Meddens, A. F. G. van der Meer, D. Oepts, and M. J. van der Wiel, "Status of the Dutch free electron laser for infrared experiments," *Nucl. Instrum. Methods*, vol. A285, pp. 67-70, 1989.
[12] P. W. van Amersfoort, R. W. B. Best, C. A. J. van der Geer, W. J. Mastop, B. J. H. Meddens, A. F. G. van der Meer, and D. Oepts, "The Felix project status report, April 1988," Rijnhuizen Rep. 88-176; "The Felix project status report, October 1988," Rijnhuizen Rep. 88-180.
[13] D. W. Feldman, R. W. Warren, B. E. Carlsten, W. E. Stein, A. H. Lumpkin, S. C. Bender, G. Spalek, J. M. Watson, L. M. Young, J. S. Fraser, J. C. Goldstein, H. Takeda, T.-S. F. Wang, K.-C. D. Chan, B. D. McVey, B. E. Newnam, R. A. Lohsen, R. B. Feldman, R. K. Copper, W. Joel, D. Johnson, and C. A. Brau, "Recent results from the Los Alamos free-electron laser," *IEEE J. Quantum Electron.*, vol. QE-23, pp. 1476-1487, 1987.

D. Oepts, photograph and biography not available at the time of publication.

W. B. Colson, photograph and biography not available at the time of publication.